Journal of Power Sources 195 (2010) 7375–7379

Contents lists available at ScienceDirect

Journal of Power Sources

journal homepage: www.elsevier.com/locate/jpowsour

Short communication

A promising $NiCo_2O_4$ protective coating for metallic interconnects of solid oxide fuel cells

Bin Hua, Wenying Zhang, Juan Wu, Jian Pu*, Bo Chi, Li Jian

School of Materials Science and Engineering, State Key Laboratory of Material Processing and Die & Mould Technology, Huazhong University of Science & Technology, Wuhan, Hubei 430074, PR China

ARTICLE INFO

Article history:
Received 28 April 2010
Accepted 5 May 2010
Available online 17 June 2010

Keywords:
Solid oxide fuel cell
Metallic interconnect
Coating
Spinel
Area specific resistance

ABSTRACT

The $NiCo_2O_4$ spinel coating is applied onto the surfaces of the SUS 430 ferritic stainless steel by the sol–gel process; and the coated alloy, together with the uncoated as a comparison, is cyclically oxidized in air at 800 °C for 200 h. The oxidation behavior and oxide scale microstructure as well as the electrical property are characterized. The results indicate that the oxidation resistance is significantly enhanced by the protective coating with a parabolic rate constant of 8.1×10^{-15} g^2 cm^{-4} s^{-1}, while the electrical conductivity is considerably improved due to inhibited growth of resistive Cr_2O_3 and the formation of conductive spinel phases in the oxide scale.

1. Introduction

The interconnect is a critical stack component of solid oxide fuel cells (SOFCs), which provides electrical connection between adjacent cells, physically separates the oxidant and fuel gases and distributes the gases to electrodes. The reduction of operating temperature of SOFCs to below 800 °C makes it possible to use metallic alloys as the interconnect materials with advantages of easy fabrication, low cost, high electric/thermal conductivity and robust structure integrity [1–4]. Among these alloys, Cr_2O_3-forming ferritic stainless steels are the frequently selected candidates due to close match of their coefficients of thermal expansion (CTE) to those of the cell components [5–8]. However, the thermally grown Cr_2O_3 oxide scale upon SOFC operation increases the electrical resistance of the interconnect to an unacceptable level during the expected service lifetime of SOFCs even at reduced temperatures, and consequently degrades the performance of SOFC stacks [9,10]. Furthermore, the volatile Cr species, primarily in the form of CrO_3 or $CrO_2(OH)_2$, generated from Cr_2O_3 tends to deposit on the surface of cathode and/or the interface between cathode and electrolyte, leading to a significant decrease in cathode activity and subsequent the stack performance [11–13]. This phenomenon is known as cathode Cr-poisoning, which is an unsolved issue accompanying applications of Cr_2O_3-forming ferritic stainless steels in SOFC cathode environment. Additionally, the volatile Cr species reacts with the glass-sealing materials, which causes stack performance degradation by increasing the leak rate of reactant gases [14,15]. The double-layer oxide scale structure of $(Mn, Cr)_3O_4$ spinel on top of Cr_2O_3, formed on Cr_2O_3-forming ferritic stainless steels, typically SUS 430 and Crofer22 APU, may offer some protection in terms of the Cr-poisoning due to the lower volatility of Cr in the spinel than in pure Cr_2O_3 [16–18]. However, Cr vaporization from $(Mn, Cr)_3O_4$ spinel may still result in an unacceptable degradation in cell performance, and further improvement against the Cr-poisoning is still necessary [19].

Surface modification via application of a protective coating of conductive oxides is an effective approach to enhance oxidation resistance, surface stability, scale adhesion and conductivity as well as alleviate Cr vaporization [19–23]. It is expected that the coating will be highly dense, electronically conductive, less volatile and thermally and chemically compatible with adjacent cell components. Perovskite ceramics have been considered as the coating due to their high electrical conductivity; however, the performance of such coatings is not as robust as anticipated. The perovskites used are mixed electronic–ionic conductors; oxide ions can permeate the coating to oxidize the substrate [24–26]. Generally, spinels can serve as a barrier to Cr cation migration and possess high electronic conductivity [7,19,27]; therefore, spinels that contain no Cr are favored for the coating application to meet all the requirements.

In the present study, $NiCo_2O_4$ spinel coating was developed on the surface of SUS 430 stainless steel by the sol–gel process that is readily applicable to metallic interconnects with various shapes and configurations. The microstructure and electrical property of the oxide scale formed on the coated SUS 430 alloy as well as the

* Corresponding author. Tel.: +86 27 87558142; fax: +86 27 87558142.
E-mail address: pujian@hust.edu.cn (J. Pu).

0378-7753/$ – see front matter © 2010 Elsevier B.V. All rights reserved.
doi:10.1016/j.jpowsour.2010.05.031

oxidation kinetics were characterized and reported in comparison with that of the uncoated SUS 430 alloy.

2. Experimental

Commercial SUS 430 stainless steel sheet with a thickness of l mm from Yuhang Stainless Steels Ltd. was selected for this study. The alloy contains 81.15 wt% Fe, 16.68 wt% Cr, 0.63 wt% Mn, 0.69wt% Si, 0.08 wt% C and residual amount of Ni, Al, P and S. Rectangular coupons with a dimension of 25 mm × 25 mm × 1 mm were obtained by using an electrical discharge machine, and the surfaces of the coupons were ground with silicon carbide paper up to 400 grits. The ground coupons were ultrasonically cleaned in acetone and ethanol, respectively, and dried prior to coating.

The sol–gel solution for preparing $NiCo_2O_4$ coating was made by using proportional amounts of nickel nitrate hexahydrate ($Ni(NO_3)_2{\cdot}6H_2O$), cobalt nitrate hexahydrate ($Co(NO_3)_2{\cdot}6H_2O$), citric acid monohydrate and ethylene glycol. Dip coating was conducted to apply the solution onto the surfaces of the prepared samples. Being dried in an oven, the coated coupons were heat treated in a reducing atmosphere of 5%H_2 + 95%N_2 at 750 °C for 2.5 h and then in air at the same temperature for another 2.5 h to form the desired Ni–Co spinel coating. Reducing atmosphere was employed to alleviate substrate oxidation during the formation of the spinel coating and enhance the interface adhesion.

Isothermal cyclic oxidation of the Ni–Co spinel coated samples, together with those uncoated for comparison, was performed at 800 °C in stagnant air. Total 5 thermal cycles in between room temperature and 800 °C were performed within 200 h of oxidation, and the weight gain after each thermal cycle was weighted using a Sartorius BT-25S electronic balance with an accuracy of 10^{-5} g. The crystal structure of all phases and cross-sectional and/or surface morphology of the as-coated and oxidized samples were characterized by a PANalytical X'Pert PRO X-ray diffractometer (XRD) with Cu Kα radiation and an FEI Quanta 200 scanning electron microscope (SEM) with an energy dissipation spectroscopy (EDS) attachment. The electrical property of the oxidized samples was measured using the standard four-probe dc technique at temperatures in between 500 and 850 °C in air.

3. Results and discussions

3.1. Phases and morphology of oxide scale

Fig. 1 shows the XRD pattern of an as-coated SUS 430 alloy coupon before subjecting it to the oxidation test. Other than the signal from the substrate, $NiCo_2O_4$, $(Ni,Mn,Cr)_3O_4$ and Cr_2O_3 phases were detected, which suggests that the SUS 430 alloy was oxidized with the formation of $(Ni,Mn,Cr)_3O_4$ and Cr_2O_3 during the heat treatment for coating development. Fig. 2 presents the overall surface morphology and the EDS elemental analysis of the surface coating. A homogeneous, crack free and compact oxide scale consisted of small particles on the level of nanometers was formed on the surface, containing Co and Ni from the solution and Cr, Mn and Fe from the thermal grown oxides or the substrate. According to the X-ray diffraction (Fig. 1), Fe should exist in the substrate, instead of the oxide scale; and Cr and Mn were selectively oxidized upon the establishment of the coating in the form of Cr_2O_3 and mixed spinel $(Ni,Cr,Mn)_3O_4$ located at between the substrate and the coating.

Fig. 3 compares the surface morphology and EDS result of the uncoated (Fig. 3a) and $NiCo_2O_4$ coated (Fig. 3b) SUS 430 alloy that were cyclically oxidized at 800 °C in air for 200 h. The thermal grown oxide scale on the surface of the uncoated SUS 430 alloy exhibits a loosely packed morphology and consisted of angular prism-shaped crystals with typical spinel structure. The surface

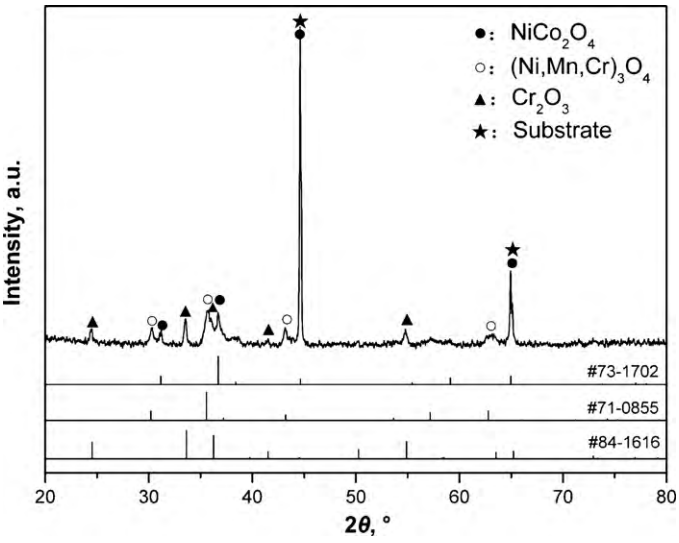

Fig. 1. XRD pattern of the as-coated SUS 430 alloy after heat treatment.

oxide is rich in Cr and Mn (as shown by the embedded EDS analysis in Fig. 3a) and most likely the $(Mn, Cr)_3O_4$ spinel. In comparison with that of the uncoated alloy, the oxidized surface of the coated SUS 430 alloy is much denser and smooth with coarse prism-shaped crystals embedded in finer well crystallized oxide particles; and no spallation is observed. The EDS analysis embedded in Fig. 3b shows that the outmost oxide scale is rich in Mn as well as Ni and Co; and the intensity of Cr is significantly decreased. This result suggests that the existence of $NiCo_2O_4$ spinel coating substantially inhibited Cr migration to excessively form Cr_2O_3 and/or $MnCr_2O_4$ on the outmost surface of the scale.

Fig. 4 demonstrates an SEM backscattering image of the cross-section and EDS line scan profile of the uncoated (Fig. 4a) and sol–gel coated (Fig. 4b) SUS 430 alloy after cyclically oxidized at 800 °C in air for 200 h. The thickness of the oxide scale of both samples is similar, in the range of 1–2 μm; however, the composition profile is different. For the uncoated, the profile embedded in Fig. 4a indicates that the scale is comprised of a Cr- and Mn-rich outer layer

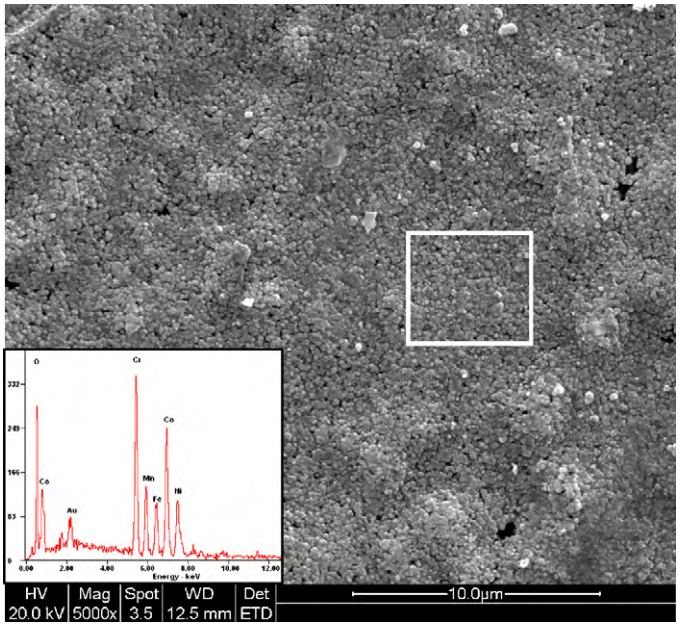

Fig. 2. Surface morphology and EDS result of the as-coated SUS 430 alloy.

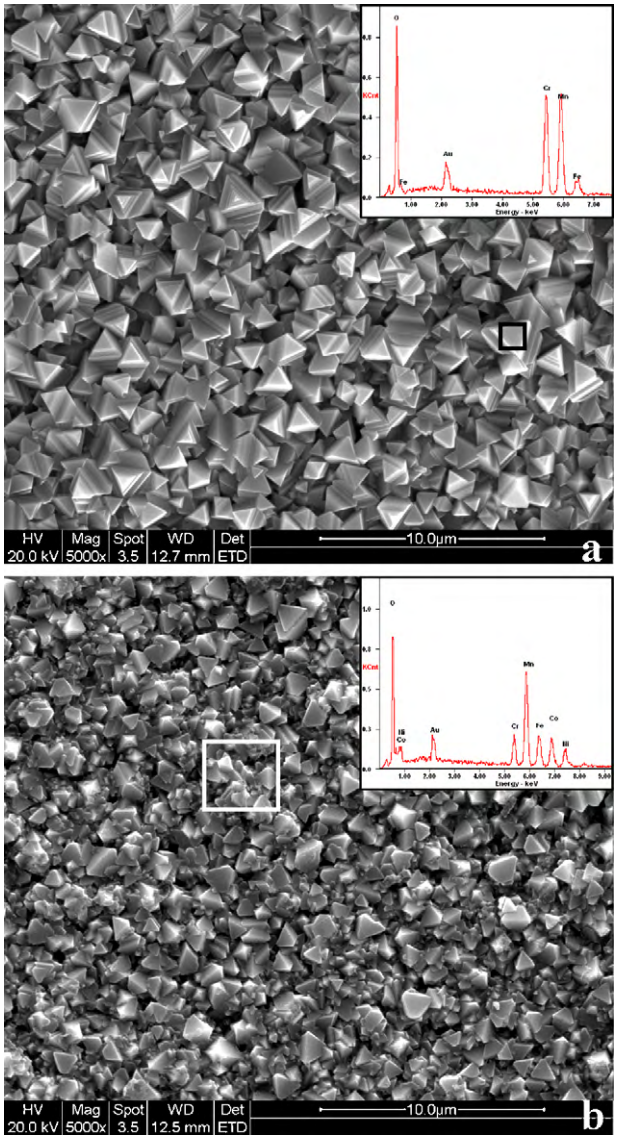

Fig. 3. Surface morphology and EDS result of the uncoated (a) and $NiCo_2O_4$ coated (b) SUS 430 alloys cyclically oxidized at 800 °C in air for 200 h.

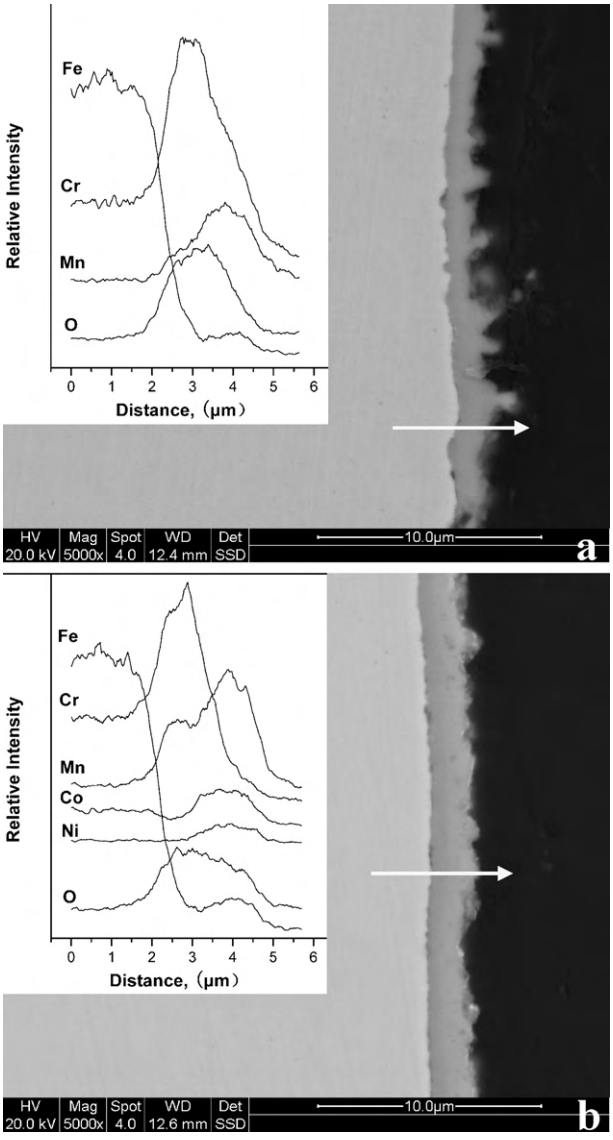

Fig. 4. Cross-section microstructure and EDS line scan profile of the uncoated (a) and $NiCo_2O_4$ coated (b) SUS 430 alloys cyclically oxidized at 800 °C in air for 200 h.

and a Cr rich inner layer adjacent to the alloy substrate, corresponding to the Mn–Cr spinel and Cr_2O_3, respectively. In the case of the uncoated, the scale is rich in Cr and Mn in the region that closes to the substrate and rich in Ni, Co and Mn on the top layer of the scale, suggesting a fast outward diffusion of Mn from the substrate into the coating $NiCo_2O_4$ during the oxidation and a possible changed coating composition of $(Ni,Mn,Co)_3O_4$.

Fig. 5 shows the XRD patterns of the $NiCo_2O_4$ coated (a) and uncoated (b) SUS 430 alloy oxidized at 800 °C in air for 200 h, respectively. The thermally grown oxide scale of the uncoated SUS 430 is comprised of $MnCr_2O_4$ spinel and Cr_2O_3 phases. Considering the morphology and EDS results, it can conclude that the oxide scale formed on the uncoated alloy demonstrate a duplex-scale structure with $MnCr_2O_4$ spinel formed on top of the Cr_2O_3 subscale. The duplex-scale was also observed by others and may be resulted from the Mn ions diffuse faster than Cr ions in Cr_2O_3 [16,17]. With $NiCo_2O_4$ coating applied onto the surface of SUS 430 alloy, the major phase in the scale is spinel, and the intensity of the diffraction peaks from Cr_2O_3 is considerably weaker than that obtained with the uncoated sample, which suggests that the growth of Cr_2O_3 during the oxidation is significantly depressed. As a result, improved

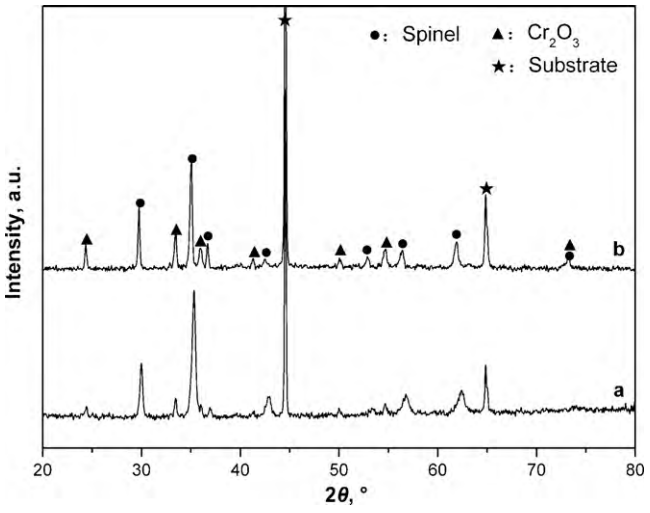

Fig. 5. XRD patterns of the $NiCo_2O_4$ coated (a) and uncoated (b) SUS 430 alloys cyclically oxidized at 800 °C in air for 200 h.

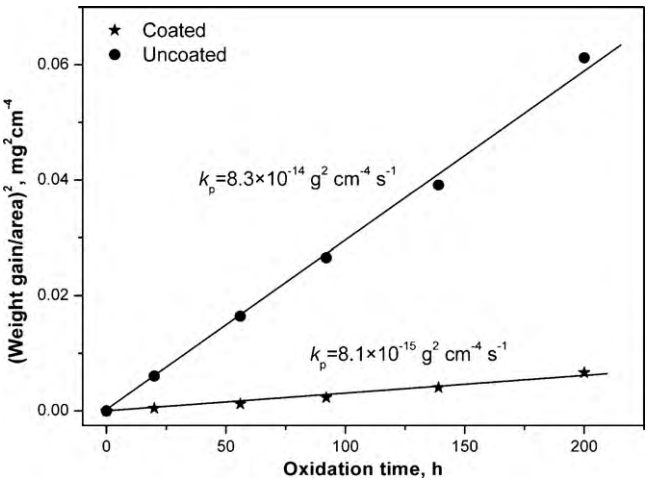

Fig. 6. Weight gain as a function of cyclic oxidation time for the $NiCo_2O_4$ coated and uncoated SUS 430 alloys at 800 °C in air.

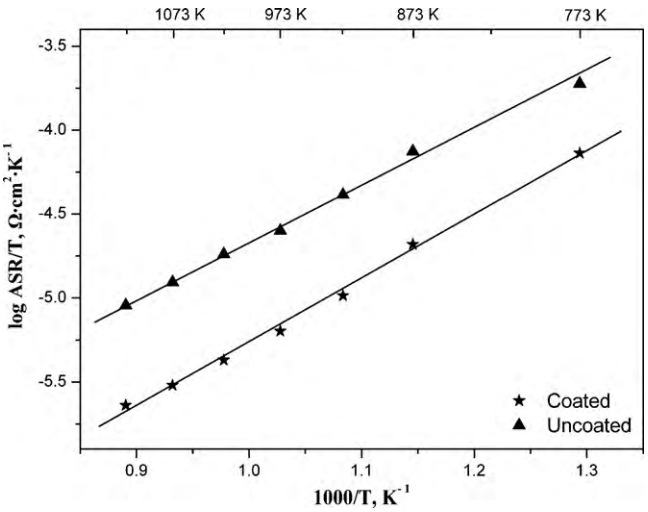

Fig. 7. ASR of the $NiCo_2O_4$ coated and uncoated SUS 430 alloys pre-oxidized cyclically at 800 °C in air for 200 h as a function of measurement temperature.

electrical conductivity and alleviated Cr evaporation are anticipated. It is also noted that the position of diffraction peaks of Cr_2O_3 and the substrate are identical to that shown in Fig. 1; however, the peak positions of the spinel in the scale are shifted towards lower angles, matching neither $NiCo_2O_4$ nor $MnCr_2O_4$ spinel. As known, the ion radius of Mn (0.08 nm) is larger than that of Ni (0.069 nm), Co (0.072 nm) and Cr (0.063 nm); increasing Mn content in $NiCo_2O_4$ or $MnCr_2O_4$ spinel will result in the shift of diffraction peaks to lower angles. Therefore, considering the EDS results in Fig. 4 and XRD in Fig. 5 together, it may be able to conclude that the outer layer of the oxide scale of the coated SUS 430 is primarily Mn-doped $NiCo_2O_4$ spinel, and the inner layer is primarily the Mn-rich $(Mn,Cr)_3O_4$ spinel. Due to the resolution limitation of the obtained XRD in Fig. 5b, the Mn-rich $(Mn,Cr)_3O_4$ and Mn-doped $NiCo_2O_4$ spinels cannot be distinguished in the present study.

3.2. Oxidation kinetics and electrical property

Fig. 6 shows the oxidation kinetics of the coated SUS 430 alloy sample cyclically oxidized at 800 °C in air, along with that of the uncoated for comparison. Total 5 thermal cycles were conducted in between room temperature and 800 °C within 200 h of oxidation. In order to understand the nature of the oxidation kinetics more explicitly, the curves in Fig. 6 are plotted as the square of the area specific weight gain against the oxidation time. As expected, the mass gain due to oxidation is increased with the oxidation time and the square of the weight gain is proportional linearly to the isothermal time, satisfying the diffusion-controlled parabolic kinetics described by

$$\left(\frac{\Delta W}{A}\right)^2 = k_p t \tag{1}$$

where ΔW is the sample weight gain, A is the sample surface area, t is the oxidation time, and k_p ($g^2\,cm^{-4}\,s^{-1}$), the parabolic rate constant, is the slope of the straight line in Fig. 6 and a measurement of oxidation resistance. The experimentally obtained k_p of the $NiCo_2O_4$ coated SUS 430 alloy is $8.1 \times 10^{-15}\,g^2\,cm^{-4}\,s^{-1}$, which is one order of magnitude lower than that of the uncoated $k_p = 8.3 \times 10^{-14}\,g^2\,cm^{-4}\,s^{-1}$, indicating that the oxidation rate is remarkably reduced by the protective coating $NiCo_2O_4$ spinel. This result is consistent with the cross-sectional observation of oxide scales. Even though the thickness of the oxide scales of both the coated and uncoated samples is almost the same, as shown in Fig. 4; however, the thermally grown oxide scale of the uncoated sample is much thicker than that of the coated one, as the original thickness of the coating is usually around 1.5 μm [22]. Previous studies [16,17] have confirmed that the oxidation kinetics of the uncoated SUS 430 alloy is controlled by the cations outward diffusion to form oxides on top of the sample surface. The access of O_2 in air to the outwardly diffused cations is limited by the $NiCo_2O_4$ protective layer.

One of the critical requirements for metallic interconnect materials is a relatively low and stable electrical resistance during SOFC operation. The area specific resistance (ASR, $m\Omega\,cm^2$), which reflects both the electrical conductivity and thickness of the oxide scale, is conventionally adopted as a measure of the electrical performance of the interconnect. Compared with the electrical resistance of the formed oxide scale, the contribution of the metallic substrate to the ASR is negligible due to its high conductivity, and the electrical property of the oxide scale determines the ASR of the interconnect. Fig. 7 shows the measured ASR of the $NiCo_2O_4$ coated and uncoated SUS 430 alloys pre-oxidized at 800 °C in air for 200 h as a function of testing temperature T. It can be seen that the ASR increases with decreasing measurement temperature and $\log(ASR/T)$ is linearly proportional to $1/T$, obeying the Arrhenius equation

$$\frac{ASR}{T} = A\,\exp\left(\frac{E_a}{kT}\right) \tag{2}$$

where A is a pre-exponential constant, E_a is the activation energy, and k is the Boltzmann's constant. The ASR of the coated alloy was lower than that of the uncoated alloy, although the total thickness of the oxide scale on coated alloy was slightly thicker than that of the uncoated alloy. The activation energy for both cases is similar, around 0.3 eV, but the pre-exponential constant, $A \approx 7.8 \times 10^{-9}$ for the uncoated and $A \approx 6.0 \times 10^{-10}$ for the coated, is significantly lowered in the case of the coated sample because of its thinner thickness of the electrically resistive Cr_2O_3 layer and higher electrical conductivity of Mn-rich Mn–Cr and Mn-doped $NiCo_2O_4$ spinels than that of Cr_2O_3 [7,19]. At 800 °C, the ASR is 3.3 $m\Omega\,cm^2$ and 13.3 $m\Omega\,cm^2$ for the coated and the uncoated alloy samples, respectively.

It is noted that the above improvement is preliminary and was achieved under the condition of only 200 h oxidation test, and further validation of the $NiCo_2O_4$ coating as a barrier for oxidation resistance and electrical conductivity enhancements of metallic interconnects needs to be performed directly in SOFC applications with the considerations of sol–gel process optimization and a longer period of testing time.

4. Conclusions

The $NiCo_2O_4$ spinel coating was applied onto the surfaces of the SUS 430 ferritic stainless steel by the sol–gel process, and both the coated and uncoated alloys were cyclically oxidized in air at 800 °C for 200 h. The oxidation behavior and the microstructure of the oxide scales as well as the electrical property were investigated. Based on the present study, the following conclusions are reached:

(1) Relatively dense and adherent $NiCo_2O_4$ spinel coating can be successful formed onto the surface of the SUS 430 alloy by the sol–gel process, which results in the formation of an oxide scale consisting of Mn-doped $NiCo_2O_4$ on the top surface, Mn-rich Mn–Cr spinel in the middle and a depressed Cr_2O_3 layer adjacent to the substrate after cyclical oxidation at 800 C in air for 200 h.
(2) $NiCo_2O_4$ protective coating can significantly increase the oxidation resistance of the SUS 430 alloy by limiting the access of O_2 in air to the outwardly diffused cations. The parabolic rate constant of the oxidation kinetics is $8.1 \times 10^{-15}\ g^2\ cm^{-4}\ s^{-1}$ for the coated specimen, in comparison with $8.3 \times 10^{-14}\ g^2\ cm^{-4}\ s^{-1}$ of the uncoated.
(3) The ASR is significantly lowered by the application of a $NiCo_2O_4$ coating, which is attributed to the thin thickness of an electrically resistive Cr_2O_3 layer and the formation of electrically conductive Mn–Cr and Mn-doped $NiCo_2O_4$ spinels in the oxide scale. $NiCo_2O_4$ spinel is confirmed to be a promising coating for the metallic interconnects of the intermediate temperature SOFCs.

Acknowledgments

This research was financially supported by National High Technology Research and Development Program of China (No. 2006AA03Z227) and National Natural Science Foundation of China (No. 50771048). The SEM and XRD were performed at the Analytical and Testing Center of Huazhong University of Science and Technology.

References

[1] W.Z. Zhu, S.C. Deevi, Mater. Sci. Eng. A348 (2003) 227–243.
[2] J.W. Fergus, Mater. Sci. Eng. A397 (2005) 271–283.
[3] W.Z. Zhu, S.C. Deevi, Mater. Res. Bull. 38 (2003) 957–972.
[4] Z.G. Yang, Int. Mater. Rev. 53 (2008) 39–54.
[5] B.C. Church, T.H. Sanders, R.F. Speyer, J.K. Cochran, Mater. Sci. Eng. A452–453 (2007) 334–340.
[6] J. Rufner, P. Gannon, P. White, M. Deibert, S. Teintze, R. Smith, H. Chen, Int. J. Hydrogen Energy 33 (2008) 1392–1398.
[7] S.J. Geng, J.H. Zhu, J. Power Sources 160 (2006) 1009–1016.
[8] J. Froitzheim, G.H. Meier, L. Niewolak, P.J. Ennis, H. Hattendorf, L. Singheiser, W.J. Quadakkers, J. Power Sources 178 (2008) 163–173.
[9] T. Horita, Y.P. Xiong, K. Yamaji, N. Sakai, H. Yokokawa, J. Electrochem. Soc. 150 (2003) A243–A248.
[10] Z.G. Yang, M.S. Walker, P. Singh, J.W. Stevenson, T. Norby, J. Electrochem. Soc. 151 (2004) B669–B678.
[11] S.P. Jiang, Y.D. Zhen, S. Zhang, J. Electrochem. Soc. 153 (2006) A1511–A1517.
[12] M. Stanislowski, E. Wessel, K. Hilpert, T. Markus, L. Singheiser, J. Electrochem. Soc. 154 (2007) A295–A306.
[13] J.W. Fergus, Int. J. Hydrogen Energy 32 (2007) 3664–3671.
[14] N.H. Menzler, D. Sebold, M. Zahid, S.M. Gross, T. Koppitz, J. Power Sources 152 (2005) 156–167.
[15] T. Horita, H. Kshimoto, K. Yamaji, N. Sakai, Y.P. Xiong, M.E. Brito, H. Yokokawa, Int. J. Hydrogen Energy 33 (2008) 3962–3969.
[16] J. Pu, J. Li, B. Hua, G.Y. Xie, J. Power Sources 158 (2006) 354–360.
[17] Z.G. Yang, J.S. Hardy, M.S. Walker, G.G. Xia, S.P. Simner, J.W. Stevenson, J. Electrochem. Soc. 151 (2004) A1825–A1831.
[18] D.E. Alman, P.D. Jablonski, Int. J. Hydrogen Energy 32 (2007) 3743–3753.
[19] Z.G. Yang, G.G. Xia, X.H. Li, J.W. Stevenson, Int. J. Hydrogen Energy 32 (2007) 3648–3654.
[20] W. Qu, J. Li, D.G. Ivey, J. Power Sources 138 (2004) 162–173.
[21] W. Qu, J. Li, D.G. Ivey, J.M. Hill, J. Power Sources 157 (2006) 335–350.
[22] B. Hua, J. Pu, W. Gong, J.F. Zhang, F.S. Lu, J. Li, J. Power Sources 185 (2008) 419–422.
[23] M. Stanislowski, J. Froitzheim, L. Niewolak, W.J. Quadakkers, K. Hilpert, T. Markus, L. Singheiser, J. Power Sources 164 (2007) 578–589.
[24] C.L. Chu, J. Lee, T.H. Lee, Y.N. Cheng, Int. J. Hydrogen Energy 34 (2009) 422–434.
[25] X. Montero, N. Jordán, J. Pirón-Abellán, F. Tietz, D. Stöver, M. Cassir, I. Villarreal, J. Electrochem. Soc. 156 (2009) B188–B196.
[26] N. Shaigan, D.G. Ivey, W.X. Chen, J. Power Sources 183 (2008) 651–659.
[27] N. Sakai, T. Horita, Y.P. Xiong, K. Yamaji, H. Kishimoto, M.E. Brito, H. Yokokawa, T. Maruyama, Solid State Ionics 176 (2005) 681–686.